Journal of Hydrology: Regional Studies 63 (2026) 103012

Contents lists available at ScienceDirect

Journal of Hydrology: Regional Studies

journal homepage: www.elsevier.com/locate/ejrh

Using hydraulic-based countermeasures to increase sediment fluxes in a reservoir desilting operation

Fong-Zuo Lee [*], Yu-Yun Tu

Department of Civil Engineering, National Chung Hsing University, 145 Xingda Rd., South Dist., Taichung City 402202, Taiwan, ROC

A R T I C L E I N F O

Keywords:
Two-dimensional numerical model
Desilting efficiency
Dredged guiding channel
Desilting tunnel
Reservoir sediment management

A B S T R A C T

Study region: This study focuses on the Nanhua Reservoir, where a two-dimensional numerical model was developed and validated to evaluate desilting efficiency under various operational strategies during Typhoon Lupit.

Study focus: The research highlights the critical role of a dredged guiding channel in enhancing turbidity concentration near the dam, which significantly improved desilting performance. The incorporation of this channel increased sediment desilting efficiency during sluicing operations. It reliably reflects turbid water transport dynamics and sediment load patterns. Simulation outcomes revealed that sediment transport time under flood mitigation operations was shortened by 5.5 hrs. The sluicing operation yielded the highest desilting efficiency of 16.47 %, while free overflow conditions had the least impact. Notably, the desilting tunnel demonstrated superior performance over the spillway for comparable outflow volumes, achieving the highest sediment concentration ratios during sluicing.

New hydrological insights for the region: Key strategies identified for maximizing sediment discharge benefits included the early activation of the desilting tunnel during high turbidity inflow events and increasing discharge rates. The sediment transport analysis indicated reduced concentrations during reservoir passage, with a strong correlation between upstream inflows and critical measurement points within the reservoir. These findings underscore the importance of integrating dredged guiding channels and optimizing desilting tunnel operations to improve sediment control during high inflow events and elevated reservoir levels. This research provides new hydraulic insights for effective reservoir sediment management, contributing to sustainable water resource management in sediment-impacted regions.

1. Introduction

Reservoir sedimentation has long posed challenges, yet it received little attention during the early 20th century when large dams were built. Demolishing dams to restore sediment balance is neither economically nor environmentally viable, highlighting the need for effective sediment management to maintain storage capacity and mitigate flood and drought risks. With climate change intensifying extreme weather events, sustainable sediment strategies are increasingly urgent to ensure the longevity and resilience of reservoirs. High-concentration sediment migration toward dams reduces water supply and storage capacity, making sediment management critical for sustainable reservoir operations (Morris and Fan, 2010; Kondolf et al., 2014). Key strategies include

* Corresponding author.
E-mail addresses: fzlee@nchu.edu.tw (F.-Z. Lee), leaf71221@gmail.com (Y.-Y. Tu).

https://doi.org/10.1016/j.ejrh.2025.103012
Received 23 January 2025; Received in revised form 27 November 2025; Accepted 30 November 2025

catchment conservation, sediment reduction, storage restoration, and adaptive operations, all requiring site-specific adaptations (Annandale et al., 2016; WRA, 2020). Upstream check dams are commonly used to trap sediment (Samad et al., 2016; Zeng et al., 2022; Zulfan et al., 2023), but fine sediments often still reach reservoirs. As a result, research increasingly emphasizes turbidity current

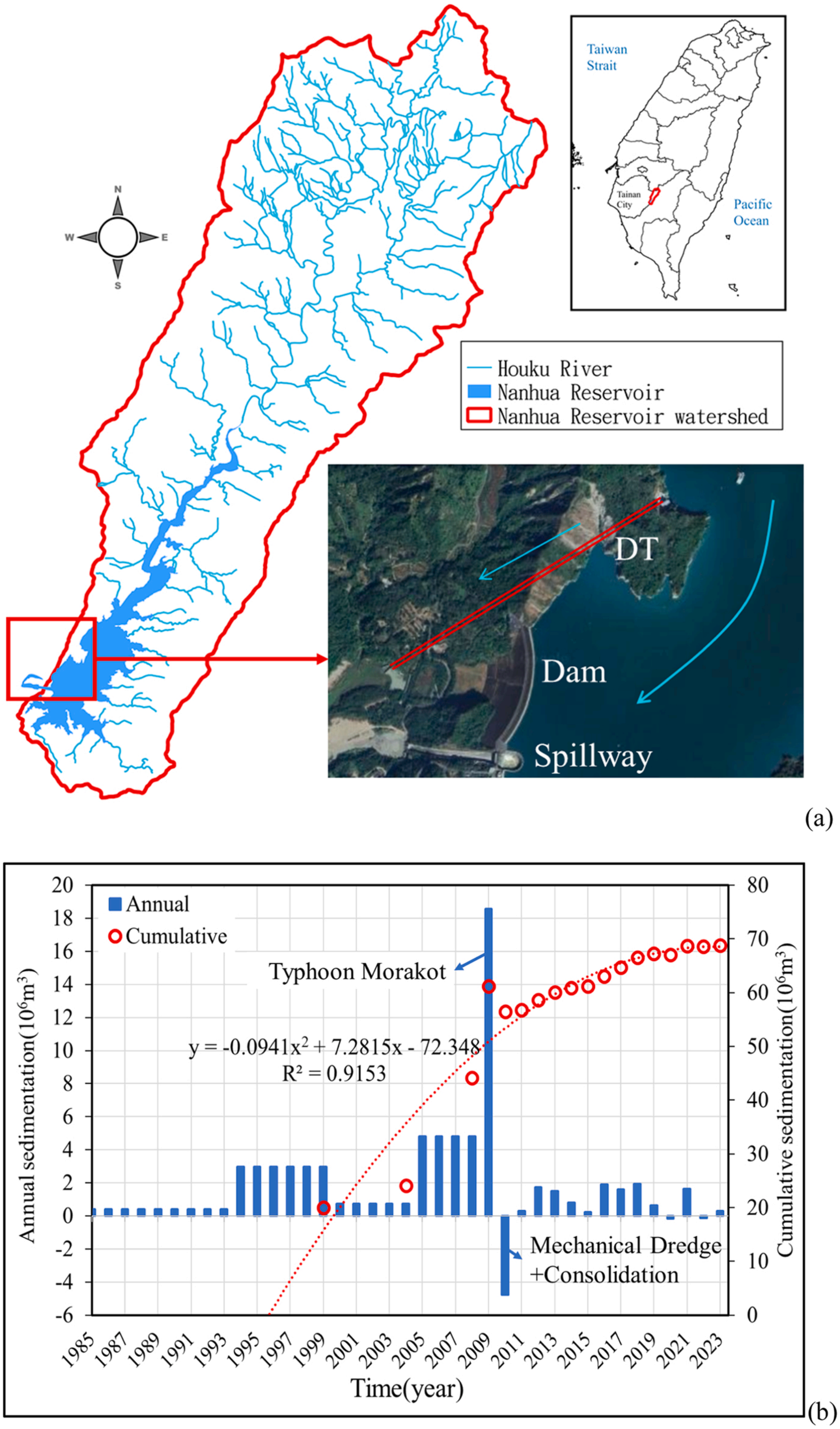

Fig. 1. Historical data in Nanhua Reservoir (a) location and watershed scope (b) sedimentation record (c) longitudinal bed profiles in various years along the thalweg.

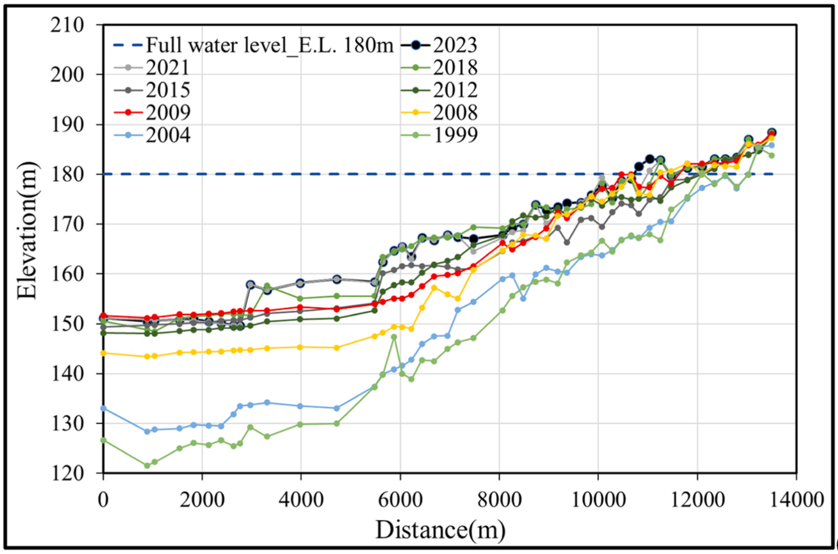

(c)

Fig. 1. (*continued*).

venting through reservoir outlets. Venting efficiency depends on outlet placement, with bottom outlets being most effective due to turbidity current stratification (Morris and Fan, 2010; Lee et al., 2014). Optimal timing, such as opening gates within 300 m of the approaching turbidity current, and favorable upstream slopes also enhance sediment evacuation (Chamoun et al., 2017, 2018; Morris and Fan, 2010).

Regular dredging extends reservoir functionality outside typhoon periods by removing accumulated sediment (Ge et al., 2021; Kantoush et al., 2021). During high-sediment events, such as typhoons, bypass tunnels allow sediment to flow downstream without settling in the reservoir (Albayrak et al., 2019; Morris, 2020). These methods mitigate sedimentation impacts, improve water quality, and support long-term reservoir sustainability. Artificial countermeasures, or guiding structures, are also being developed to optimize sediment removal. For example, in Morocco's Oued Neckar Reservoir, turbidity currents were directed toward bottom outlets using submersible dikes and guide embankments (Batuca & Jordaan, 2000). Studies on solid and permeable obstacles show they can redirect turbidity currents and reduce sediment deposition near dams (De Cesare et al., 2006; Oehy and Schleiss, 2007; Baghalian and Ghodsian, 2020). Flushing channels, especially effective during reservoir drawdown, have demonstrated high sediment removal efficiency (Chen and Tsai, 2017; WRA, 2020; Wang et al., 2020; Esmaeili et al., 2021; Lai et al., 2024). The "main-channel characteristic" approach has been applied to enhance sediment transport even at high water levels (Chen, 2022; Imtiyaz et al., 2024). However, flushing channel performance varies with hydrological conditions, requiring flexible design (Wang et al., 2020; Lee and Huynh Nguyen, 2024). To address this, our study proposes incorporating a dredged guiding channel aligned with potential flushing areas to concentrate and accelerate sediment flow, enhancing sediment transportation and improving long-term reservoir capacity and operational efficiency.

Numerical modeling is crucial for studying reservoir desiltation, especially since field observations of turbidity currents during flood events are difficult (Robb et al., 2021; Lee et al., 2024; Lee and Du, 2025). Hydrodynamic and sediment transport models, using two-dimensional (2D) or three-dimensional (3D) simulations, are essential for analyzing sediment dynamics. While 3D models offer detailed predictions, their high computational demands limit routine use. In contrast, 2D models balance accuracy and efficiency, making them practical for evaluating bottom outlet sluicing under various scenarios, provided they are carefully calibrated.

A review of recent studies confirms the effectiveness of 2D modeling for simulating turbidity currents and guiding sediment management strategies. Hu et al. (2012) and Huang et al. (2019) demonstrated that 2D models can predict turbidity current behavior and optimize sluicing operations. Anari et al. (2020) emphasized the suitability of 2D models for capturing sediment dynamics near sluice gates. Research by Chen (2020), (2022) and Imtiyaz et al. (2024) used 2D models to assess sediment concentration and desilting efficiency in bottom-dredged channels. Wang et al. (2020) proposed a 2D simulation-based reservoir partitioning strategy to improve flushing efficiency, while Chen and Tsai (2017), Imtiyaz et al. (2024), and Lee and Huynh Nguyen (2024) showed that narrow gorge-shaped channels enhance desilting. 2D models have also been applied to evaluate the impact of hydraulic structures on flow and sediment deposition (Lee et al., 2021; Hung et al., 2022; Sun et al., 2023). More recently, studies by Lee et al. (2023) and Lee and Huynh Nguyen (2024) analyzed the role of main flushing channels in mitigating sedimentation under steady conditions. Collectively, these studies highlight the practical value of 2D modeling in designing efficient desilting strategies for diverse operational scenarios.

2. Methods

2.1. Study site

The Nanhua Reservoir is situated in Nanhua District, Tainan City, Taiwan, upstream of the Houku River, a tributary of the Zengwen River (as shown in Fig. 1(a). Completed in 1993, its water sources include the Houku River and the Jiasian Weir, a tributary of the Gaoping River. The reservoir was designed to cover a watershed area of 108.30 km^2, with an initial storage capacity of 150 million m^3 . It comprises four primary structures: the dam, spillway, and water intake. The dam is a central-zone rolled earth-rock structure with a top elevation of 187.5 m and a full water level of 180 m. The spillway features an ungated U-shaped, free-flow weir with a top elevation of 180 m, while the water intake is an inclined tower with four intake ports positioned at elevations of 170, 157, 144, and 131 m.

Taiwan's geological and climatic conditions—steep topography, tectonic activity, fragile geology, and heavy precipitation—contribute to its reputation as the world's leading sediment producer. The Nanhua Reservoir experiences significant sedimentation, primarily due to typhoon-induced landslides and torrential rains (as shown in Fig. 1(b). Sedimentation data presented in 2024 show that the cumulative deposition volume reached 295.4 Mm^3 , reducing the reservoir's capacity to 60.53 % of its initial design. Despite an existing capacity of 453 Mm^3 , sediment yields from upstream watersheds, exacerbated by typhoon flood events, have caused considerable sediment accumulation over the decades.

Typhoon Morakot (August 7–9, 2009) was particularly destructive among these events. Its prolonged movement during landfall and post-landfall phases caused intense rainfall, resulting in sediment accumulation up to EL—179.1 m in the reservoir bed. Field surveys reveal significant longitudinal bed variation over time, as shown in Fig. 1(c), with sediment forming a planar depositional pattern near the dam site in recent years. To address sedimentation, a desilting tunnel was planned in 2011, with construction beginning in 2015 and completion in 2021. The tunnel includes a water entrance, shaft, gate, tunnel, and energy-dissipating outlet. The entrance, a rectangular cross-section measuring 15 m wide and 9.5 m high, provides a flow area of 142.5 m^2. The tunnel can discharge 1000 m^3 /s and has a diameter of 9.5 m. Its outlet connects to the original river channel to dissipate energy effectively. However, despite its operation during Typhoons Lupit in 2022 and 2023, the reservoir's capacity declined, decreasing from 89.35 million m^3 in 2021–89.20 million m^3 in 2023 (Taiwan Water Corporation Sixth Branch, 2023a).

Given water resource conservation and supply constraints, the reservoir prioritizes maximizing storage capacity during flood events. However, annual dredging near the intake is insufficient to maintain capacity. Therefore, a comprehensive management approach is essential, integrating sediment routing and dredging techniques to manage flood-induced turbidity currents. Strategies such as constructing a dredged guiding channel to route turbidity currents aim to enhance venting efficiency. This study examines improved desilting performance using dredged guiding channels (Imtiyaz et al., 2024; Lee and Huynh Nguyen, 2024). A two-dimensional (2D) layer-averaged model developed by Lai (2015) has been employed to simulate turbidity current venting through the reservoir outlets (Lai et al., 2015; Huang et al., 2019; Huang, 2024).

2.2. 2-D Numerical methodology

Two-dimensional (2D) models are invaluable for reservoir and water managers, providing detailed topographies and flow feature simulations. The Sedimentation and River Hydraulics (SRH-2D) model is particularly effective for describing two-dimensional hydraulic and sediment transport processes (Wang et al., 2020; Huang et al., 2019). This model can simulate a wide range of flow conditions—steady, quasi-steady, or unsteady—and sediment transport in cohesive and non-cohesive states. It also offers options for multi-size sediment transport with bed sorting and armoring (Lai, 2010). The SRH-2D model predicts bed changes by tracking non-equilibrium sediment transport for suspended, mixed, and bed loads, applicable to various bed types, including granular, erodible rock, and non-erodible surfaces, and can also simulate bank erosion (Lai, 2017).

Lai et al. (2015) later developed a 2D layer-averaged turbidity current model for reservoir turbidity current simulations. Huang (2024) and Hung et al. (2022) applied this model in field cases. The model solves hydraulic mechanisms using mass conservation and momentum equations and simulates turbidity current transport using non-equilibrium sediment transport equations (as shown in Eqs. 1 and 2). Lai et al. (2015) and Huang et al. (2019) describe detailed numerical methods.

$$\frac{\partial h_t C_{kt}}{\partial t}+\frac{\partial h_t U C_{kt}}{\partial x}+\frac{\partial h_t V C_{kt}}{\partial y}=w_{kt}(p_{kt}E_{kt}-C_{bk}) \tag{1}$$

$$(1-\gamma_b)\frac{\partial Z_{bt}}{\partial t}=-\sum\nolimits_k w_{kt}(p_{kt}E_{kt}-C_{bk}) \tag{2}$$

Where, h_t : turbidity current thickness; C_{kt}: layer-averaged volumetric concentration of the k_{th} sediment size class; t: time; x and y: x- and y-direction in Cartesian coordinates; U and V: velocity in the x- and y-directions; U_{av}: average velocity defined as $\sqrt{U^2+V^2}$;; w_{kt}: fall velocity of the k_{th} sediment size class; p_{kt}: volume fraction of the k_{th} sediment size class; E_{kt}: erosion rate potential; C_{bk}: near-bed concentration of the k_{th} size class; γ_b: porosity of bed sediment; Z_{bt}: bed elevation.

The layer-averaged concentration is used to calculate the near-bed concentration (C_{bk}). The relationship between C_{bk} and the shape factor of sediment particle r_{0k} is $C_{bk}=r_{0k}C_k$ (García, 1994), and the shape factor is computed by:

$$r_{0k}=1.64+0.4\left(\frac{d_k}{d_{gm}}\right)^{1.64};\ (d_{gm})=\frac{\sum C_{kt}\ ln(d_k)}{\sum C_{kt}} \tag{3}$$

Where, d_k = diameter of sediment size k ; d_{gm} = the geometric mean diameter ; The erosional rate potential (E_{kt}) is based on the equation of Engelund and Hansen (Engelund and Hansen, 1972). It is widely used in streams and reservoirs for fine sediment transport and is suitable for field-scale applications, it may be expressed as:

$$E_{kt} = 0.05 m_E \frac{\sqrt{U^2 + V^2}}{h_t \sqrt{\frac{(s-1)g}{d_k}}} \left[\frac{V_*^2}{(s-1) g d_k} \right]^{1.5} \tag{4}$$

When suspended sediment flows, deposition or erosion occurs as the concentration approaches equilibrium. The SRH-2D model uses two adaptation coefficients—the deposition and the erosion coefficients—to simulate this process, ensuring the accurate representation of suspended sediment transport and concentration equilibrium. In the SRH-2D mobile bed model, the governing equations for achieving sediment concentration equilibrium during deposition or erosion are calculated as follows:

$$S_e = \frac{q_s^* - q_s}{L_s} \tag{5}$$

$$L_s = (1 - fL_b) + \frac{\lambda U_{av} h_l}{w_{kt}} \tag{6}$$

Where S_e = unit sediment equilibrium transport rate ; q_s^* = local sediment transport capacity ; q_s = sediment transport flux advected into the local area from upstream. ; L_s = distance of suspended sediment transport, known as adaptation length ; f is the load parameter representing the probability for the sediment to be suspended; L_b is the bed load adaptation length; λ = user-specified parameter for net deposition and erosion. Default values for the two adaptation coefficients are 0.25 and 1.0 for deposition and erosion, respectively. h_l = local water depth.

2.3. Boundary conditions

The preprocessing steps for the numerical model involved managing terrain data and creating the 2D simulation grid file needed for SRH-2D simulations with the SMS software (Surface-water Modeling System, v.13.0). The simulation area covers a range from the upstream Guanshan No. 9 Bridge in the reservoir (Section 48) to the dam site. Guanshan No. 9 Bridge serves as the inflow boundary, while the downstream outflow boundaries include the Desilting Tunnel (DT) outflow, the spillway (SW) free overflow, and the water intake at 151 m. The grid density for the reservoir area is between 40 and 50 m, following Hung et al.'s (2022) recommendation. The time step is set between 0.1 and 1.0 s, with a grid count below 20,000. To interpolate terrain elevations in unmeasured areas within each grid cell, the Inverse Distance Weighting (IDW) method was applied based on known elevation data for the reservoir. Based on grain size, Manning's roughness coefficient, as indicated in Table 1, is set to 0.006. The grain size distribution is derived from suspended load samples collected at Guanshan No. 9 Bridge (Taiwan Water Corporation Sixth Branch, 2021). The grain size of d_{30} is 0.075 mm, d_{50} is 0.093 mm, d_{75} is 0.215 mm, and d_{90} is 0.361 mm, respectively. Fig. 2 provides a detailed setup of the 2D numerical model for Nanhua Reservoir, illustrating terrain elevations, boundary conditions, and key sediment observation points.

Based on the field measurement during Typhoon Lupit in 2021 (Taiwan Water Corporation Sixth Branch, 2021), the suspended sediment concentration could be related to the inflow discharge as the following regression formula.

$$Q_s = aQ^m = 11.30 Q^{1.89}, \ \mathrm{R}^2 = 0.90 \tag{16}$$

where a and m are the coefficients of the regression relationship; Q_s is inflow sediment discharge (ton/day);Q is inflow discharge (m^3/s).

2.4. Study cases

The Nanhua Reservoir was initially designed with a free overflow spillway without a gated discharge control. Besides the spillway in front of the dam and the desilting tunnel located on the right bank in the reservoir's midsection, there are no additional flood discharge or bottom outlet facilities to assist with hydraulic desilting. This limited infrastructure has contributed to a gradual reduction in the reservoir's capacity when desilting operations are insufficient. To improve hydraulic desilting efficiency while maintaining the reservoir's storage and water supply functions, assessing and enhancing the discharge facilities to balance sediment inflow and outflow is essential.

During Typhoon Lupit in 2021, operational observations (Table 2) showed that although high sediment concentrations above 10,000 PPM were measured near the desilting tunnel entrance at Section 13, the concentration at the tunnel's discharge outlet was significantly lower. Several factors can explain this reduction. At the time, the reservoir water level was over 180 m, causing sediment-

Table 1
Grain size distribution.

Diameter Distribution	D_{10}	D_{30}	D_{50}	D_{65}	D_{75}	D_{90}	D_{100}
Grain size (mm)	0.0130	0.0750	0.0932	0.1416	0.2151	0.3606	1.2409

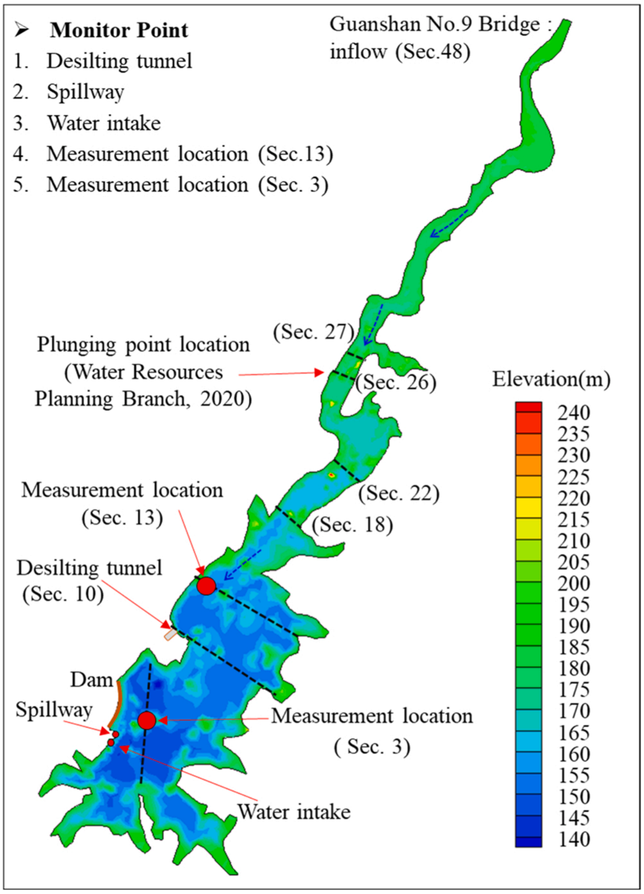

Fig. 2. Boundaries and measurement locations.

Table 2
Typical event for the discussion of with/without dredged guiding channel.

Events	Year	Total precipitation (mm)	Rainfall intensity (mm/hr)	Inflow volume (10^6 m^3)	Peak inflow discharge (m^3/s)	Initial water level (m)	Max outflow discharge (m^3/s)
Typhoon Lupit	2021	731	34.0	68.8	577	180.22	436

laden water from the free overflow at the dam to flow toward the downstream area. The desilting tunnel was only partially open, limiting the impact of the pressure flow field. After passing Section 13, the reservoir cross-section widens, resulting in sediment diffusion and dilution. Additionally, changes in the slope of the reservoir upstream of the desilting tunnel entrance have altered the flow path, shifting the high sediment concentrations observed at Section 13 toward the reservoir's central cross-section. Consequently, only part of the sediment load is discharged through the desilting tunnel.

To regulate reservoir operation strategies, this study employs a validated two-dimensional numerical model (detailed in the

Table 3
Scenarios of four reservoir operation strategies under Typhoon Lupit hydrograph.

Cases	Operation condition	Initial water level (m)	Cases	Operation condition	Initial water level (m)	Cases	Operation condition	Initial water level (m)
C-1	Free overflow	175.5	C-5	Free overflow	177.5	C-9	Free overflow	180.5
C-2	Downstream replenishment sediment flushing		C-6	Downstream replenishment sediment flushing		C-10	Downstream replenishment sediment flushing	
C-3	Sluicing operation		C-7	Sluicing operation		C-11	Sluicing operation	
C-4	Flood mitigation		C-8	Flood mitigation		C-12	Flood mitigation	

previous section) to design various water release strategies tailored to specific operational objectives. These strategies are developed for different initial water levels—high, medium, and low—and include scenarios focused on "free overflow," "downstream replenishment sediment flushing," "sluicing operation," and "flood mitigation". Simulations are conducted to assess the effectiveness of hydraulic desilting under each strategy. The historical flood event from Typhoon Lupit in 2021 is the basis for this analysis. Using the operational optimization model (Taiwan Water Corporation Sixth Branch, 2023b), reservoir water levels and discharge flow rates across various facilities were calculated for the four operational strategies. The initial reservoir water levels were 175.5, 177.5, and 180.5 m. Scenarios for each operation strategy at the Nanhua Reservoir were designed, encompassing peak inflow rates, peak sediment inflow rates, and case analyses, as shown in Table 3. With three initial reservoir water levels for each strategy, 12 simulation scenarios were generated to discuss the effect of with/without dredged guiding channels. The inflow hydrograph from Typhoon Lupit was used to establish boundary conditions, depicted in Fig. 3. Key aspects of each strategy scenario include:

Free Overflow: In this scenario, the desilting tunnel remains closed, and water is only released via free overflow at the spillway, beginning at the 71st hour and continuing to the end of the simulation. The peak discharge rate reaches 414 m^3 /s, with a steady intake of 12 m^3 /s.

Downstream replenishment sediment flushing: The desilting tunnel opens in the 55th hour, initially discharging 100 m^3 /s. Between the 56th and 96th hour, the discharge increases to 300 m^3 /s while maintaining a constant intake of 12 m^3 /s.

Sluicing Operation: The desilting tunnel opens at the 2nd hour, maintaining an initial discharge of 50 m^3 /s. Between the 75th and 77th hour, the discharge rate increases to 300 m^3 /s, rising to 550 m^3 /s between the 78th and 83rd hour and reaching 800 m^3 /s between the 107th and 108th hour, with a consistent water intake of 12 m^3 /s.

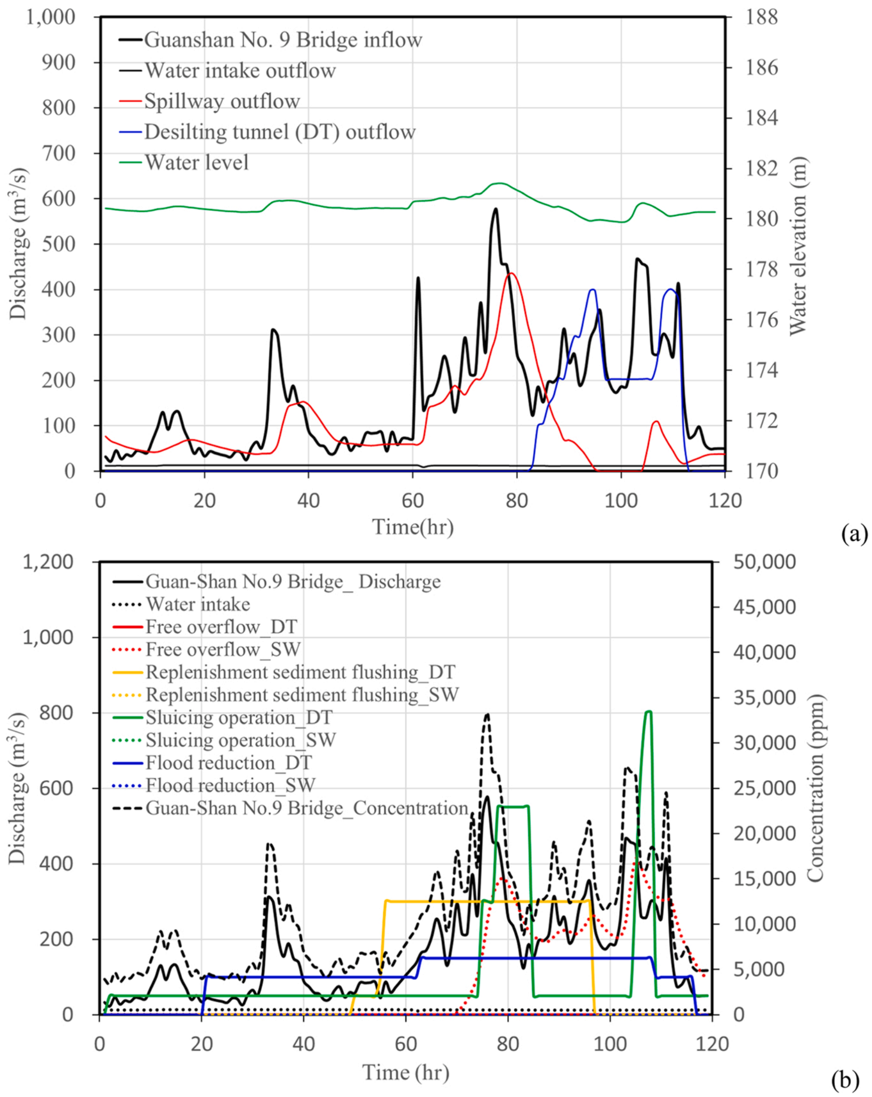

Fig. 3. Boundary conditions of (a) Typhoon Lupit (b) Scenarios of four reservoir operation strategies.

Flood mitigation: In this scenario, the desilting tunnel opens from the 21st to the 116th hour, with discharge rates ranging from 100 to 150 m^3 /s. The water intake remains steady at 12 m^3 /s.

Each scenario provides insights into water resource conservation strategies, sediment desolation management, and reservoir flood control.

3. Results and discussion

3.1. Results of Model calibration and verification

The measured sediment concentration of the outflow during this event was used to validate the model. During the turbidity current simulation, the 2DLAM model simulated and output sediment concentration hydrographs at the desilting tunnel and water intake points. The parameters for the two-dimensional simulation and validation of the Nanhua Reservoir are detailed in Table 4. The validation used data from an actual Typhoon event (Lupit) and two hydraulic model test cases (Typhoon Kalmaegi and a 25-year (Q_{25}) return period event) (Taiwan Water Corporation Sixth Branch, 2023b; WRA, 2014; Lee and Du, 2025). Validation results for measurement locations and outflows are shown in Fig. 4.

The time difference between the upstream inflow peak and downstream outflow sediment concentration peak estimates the sediment transport time from upstream inflow to the measurement points and outflow facilities (Fig. 4a, b). During Typhoon Lupit, sediment concentration reached Sec. 13, DT, and Section 3 at approximately the 24th, 36th, and 89th hours, respectively. A comparison of observed and simulated sediment concentrations at various points showed that the overall trends and sediment transport behavior were consistent despite minor differences in values and delay times. Fig. 4(c) highlights the substantial agreement between simulated and measured data in Sec. 13 and Section 3.

The study also analyzed the sediment load from the desilting tunnel, calculated cumulative and desilting efficiency (total outflow sediment load/total inflow sediment load), and compared them to simulation results (Fig. 4b, d). During Typhoon Lupit, the cumulative outflow sediment load was 65,005 tons, with a desilting efficiency of 5.83 %. The simulated load was 83,182 tons, with an efficiency of 7.46 %, yielding an error of 1.63 %. For Typhoon Kalmaegi, sediment discharge reached 1815,412 tons with a sediment discharge ratio of 24.89 %, while the 25-year return period event produced 1349,147 tons with a ratio of 25.09 %. Validation results revealed that hourly sediment concentration values differed slightly between measurements and simulations, and cumulative outflow sediment loads were highly consistent. Errors between measured and simulated outflow sediment loads were 1.63 %, 0.63 %, and −1.01 % for Typhoon Lupit, Typhoon Kalmaegi, and the 25-year return period event, respectively. These findings align with previous studies (Lai et al., 2015; Huang et al., 2019; Hung et al., 2022; Lee and Du, 2025), confirming the accuracy of the sediment discharge simulations.

Additionally, the simulated desilting efficiency of the sediment prevention tunnel in the two-dimensional model ranged from 7.46 % to 25.09 % (Fig. 4d), demonstrating a positive correlation with inflow and sediment inflow volumes. These results provide valuable insights into sediment transport dynamics and sediment management strategies within the reservoir.

3.2. Results of dredged guiding channel performance

To investigate the impact of forming a primary deep channel through dredging on sediment transport and discharge rates in the Nanhua Reservoir, this study developed a 2D simulation grid terrain with the main deep channel for the reservoir area, referred to as a bottom-guided flow channel. The dimensions and location of this bottom-guided flow channel were evaluated based on bed erosion and deposition under higher flow scenarios. The report stated, "Hydraulic Model Test of Flood and Sediment Prevention Sub-Dam and Empty Reservoir Flushing for the Nanhua Reservoir" (Taiwan Water Corporation Sixth Branch, 2017). This study simulated two empty-reservoir sediment flushing test scenarios with peak flow rates of 300 m^3/s and 600 m^3/s, both with variable flows. Only the desilting tunnel was opened for sediment discharge during the flushing process, with a total simulation time of 32 h. Fig. 5 illustrates the inflow and outflow boundary conditions for the 2D model.

The 2D simulation grid was based on the 2023 DEM data of the Nanhua Reservoir (Taiwan Water Corporation Sixth Branch, 2023a). Simulation results for bed erosion and deposition distribution at flow rates of 300 m^3/s and 600 m^3/s are shown in Figs. 6(a) and 6(b). These results were validated against the findings of the Taiwan Water Corporation Sixth Branch (2023a), showing general consistency in the shape of the flushing channel area near the desilting tunnel entrance.

The empty-reservoir flushing simulation preliminarily determined the direction and location of the main deep channel. However, confirming the precise size and location of the bottom-guided flow channel requires higher flow and extended scouring duration. Consequently, this study simulated a 1000 m^3/s steady inflow with the desilting tunnel fully open at 1000 m^3/s for 120 h. The resulting erosion and deposition distribution is illustrated in Fig. 6(c). Based on the study results of Chen (2020), Liu (2023), Imtiyaz

Table 4
Parameters of numerical simulation.

Parameters	Time step *dt* (hr)	Manning *n* value	Sediment transport equation	Turbulence coefficient C_μ	Deposition coefficient *Adept*	Erosion coefficient A_{ero}
Values	0.1	0.01	Engeland-Hansen (1972)	0.7	0.5	1.0

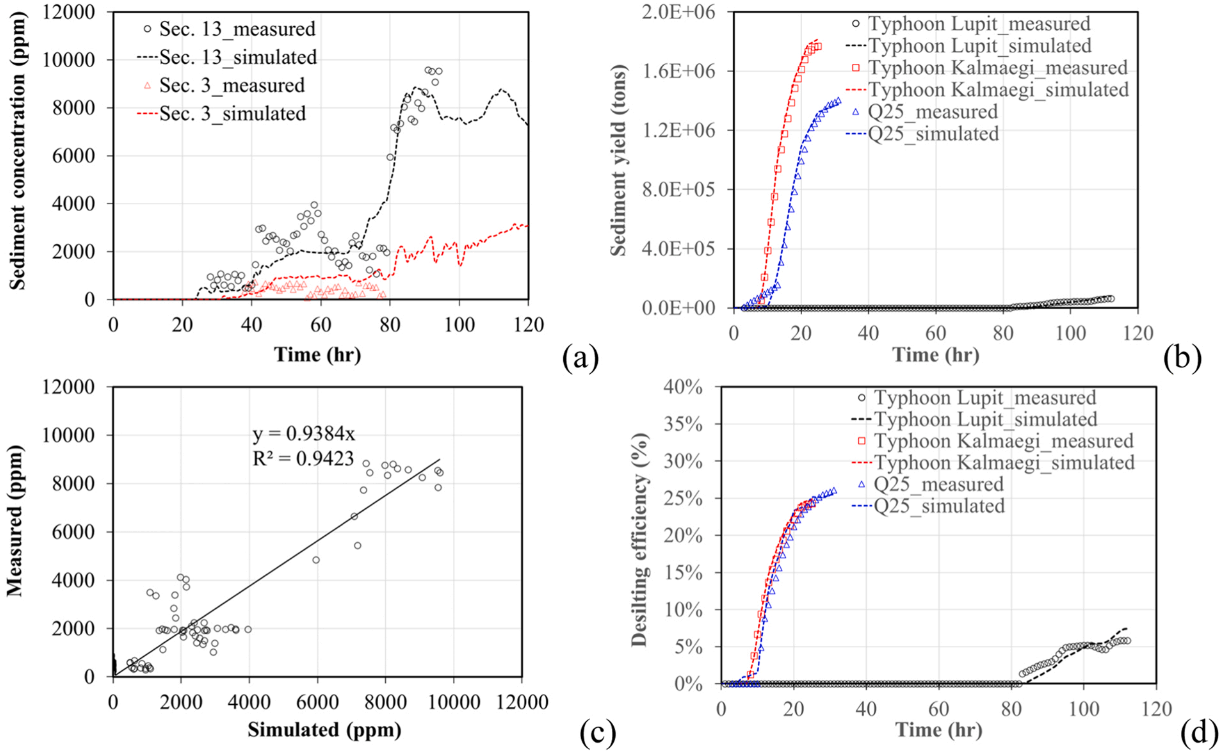

Fig. 4. Numerical model verification using Typhoon Lupit and hydraulic model tests(a) concentration comparison at measurement sections (b) sediment yield comparison at DT (c) simulated accuracy at measurement sections (d) desilting efficiency comparison at DT.

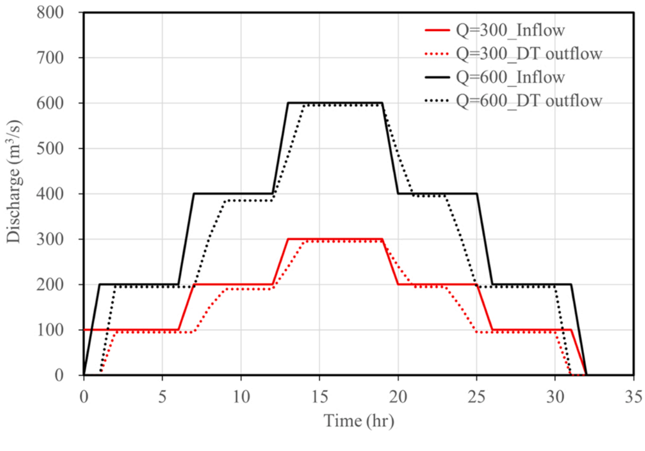

Fig. 5. Condition of empty-reservoir flushing under peak inflow rates of 300 m^3/s and 600 m^3/s.

et al. (2024), and Lee and Huynh Nguyen (2024), the dredged guiding channel, which starts from a narrow or canyon area to the entrance of the desilting tunnel, demonstrates relatively improved desilting efficiency. The geometry and channel slope, determined by the angle of repose of sediment for the side slopes of the channel, create a uniform bottom slope from the upstream end of the dredged guiding channel to the desilting tunnel entrance, forming an idealized design. Consequently, the planned bottom-guided flow channel extends from section 10 (in front of the desilting tunnel entrance) upstream to section 27, covering a length of 3816 m. Section 27, located on a relatively flat reservoir bed, connects upstream areas with steeper slopes that accommodate incoming flow and sediment.

The deep channel design addresses significant bends in the mid-reservoir "S" segment (sections 22–26), where erosion and deposition are more pronounced. The cross-sectional profile of the bottom-guided flow channel has a trapezoidal shape, wider at the top than at the bottom. The channel base width is 100 m, with 15 m side slopes on each bank, a top width of 130 m, and a slope of 0.0068, with an average depth of 9.7 m. Fig. 7 shows the layout and grid terrain for the bottom dredged guiding channel.

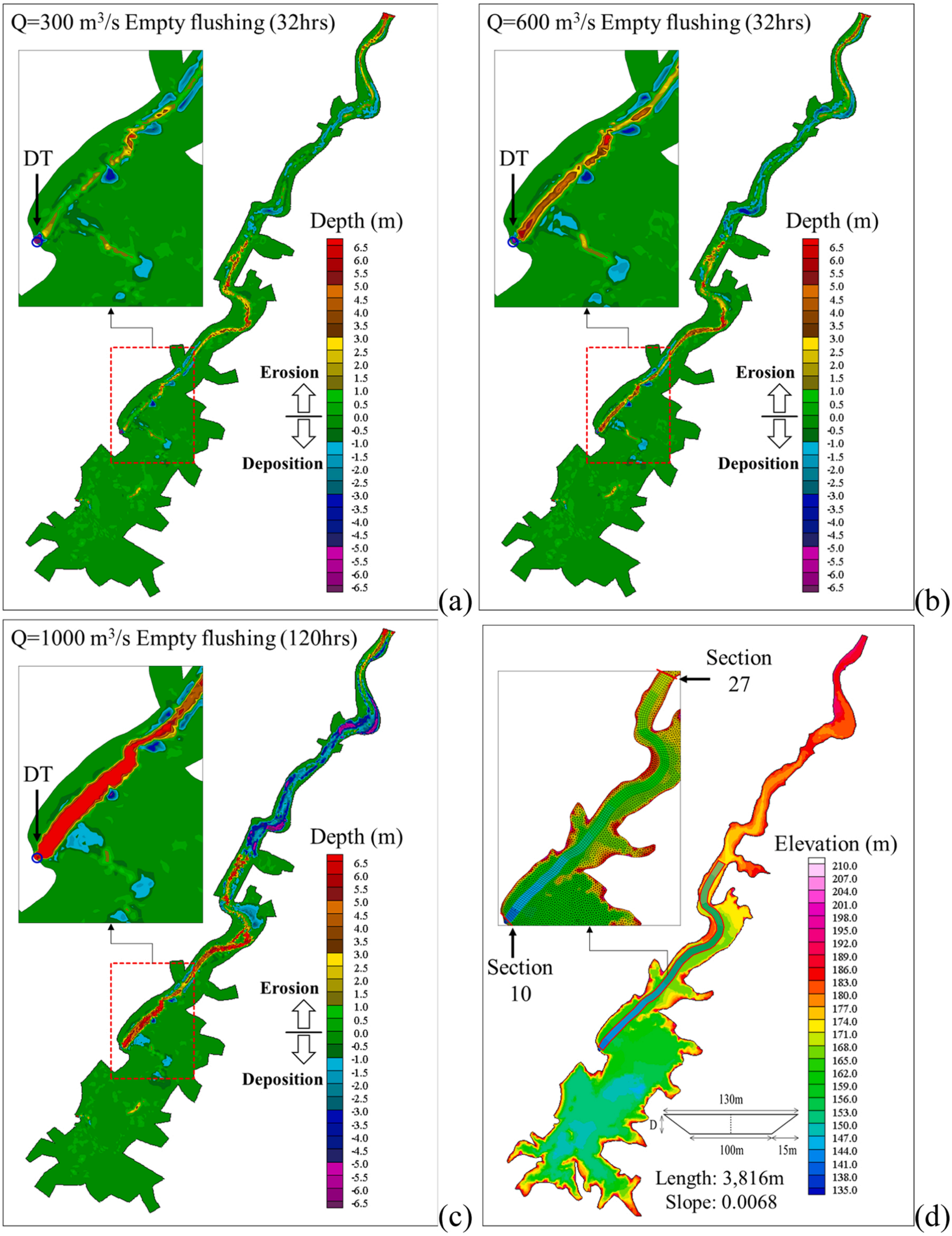

Fig. 6. Empty flushing conditions and dredged guiding channel (a) 300 m^3/s (b)600 m^3/s (c)1000 m^3/s (d) location and geometry of dredged guiding channel.

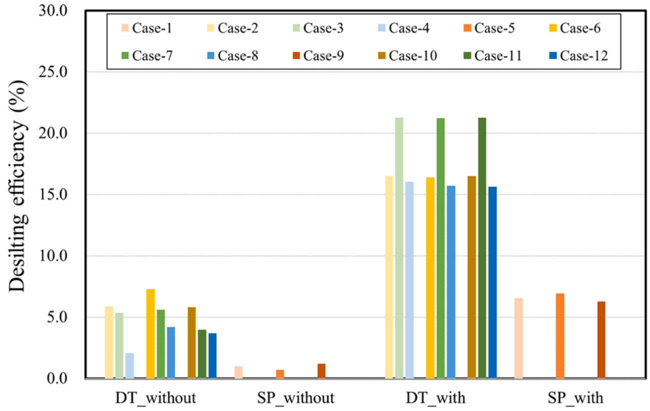

Fig. 7. Desilting efficiency comparison (with/without) of the dredged guiding channel.

3.3. Discussions

To compare the sediment transport phenomena and desilting efficiency of the Nanhua Reservoir's outlet facilities with and without a bottom-guided flow channel, this study simulated 12 operational strategies for the 2021 Typhoon Lupit event using a 2D grid terrain incorporating the bottom-guided flow channel (Fig. 7), referred to as Scenario C′. The inflow sediment concentration during Typhoon Lupit increased significantly at the first peak (33,318 ppm), which was used to establish peak sediment concentration at three monitoring points: Float No.13, the desilting tunnel entrance, and the intake tower entrance (EL.151 m) at the dam. The time series for peak sediment concentration at Guanshan No.9 Bridge was set as hour 0. Table 6 compares peak sediment concentrations and occurrence times at monitoring points with and without the bottom-guided flow channel.

When comparing the simulation results for free overflow conditions (Cases C/C′-1, 5, and 9), the average travel time of high-concentration sediment-laden water to Float No.13 decreased by approximately 2.0 h, with peak concentration increasing by around 7100 ppm. The average travel time was reduced by about 4.7 h at the desilting tunnel entrance, and peak concentration rose by approximately 8000 ppm. At the intake tower, the average travel time decreased by about 11.3 h, with an increase in peak concentration of approximately 2100 ppm.

For erosion conditions (Cases C/C′-2, 6, and 10), travel time to Float No.13 decreased by approximately 2.0 h, with a peak concentration increase of around 6100 ppm. At the desilting tunnel, travel time decreased by about 9.3 h, with a peak concentration increase of 6800 ppm, and at the intake tower, travel time was reduced by about 3.7 h, with a peak concentration rise of about 1500 ppm.

For sediment discharge scenarios (Cases C/C′-3, 7, and 11), Float No.13 showed a reduction of around 1.7 h in travel time with a peak concentration increase of about 6500 ppm. The desilting tunnel had a reduction of 4.7 h and a 7100 ppm increase, while the intake tower saw travel time reduced by 3.7 h and a peak increase of around 1400 ppm.

In Cases C/C′-4, 8, and 12, travel time to Float No.13 was reduced by about 3.0 h, with an increase in peak concentration of around 6900 ppm. The desilting tunnel travel time decreased by 5.7 h, with a 7700 ppm increase, and the intake tower travel time was reduced by 8.3 h, with an increase in peak concentration of approximately 1500 ppm.

The sediment concentration and flow velocity distributions of turbid water entering the reservoir and passing through the desilting tunnel, under terrain conditions with and without a dredged guiding channel during Typhoon Lupit, are shown in Fig. 8. The distributions for both terrain types are compared using the delayed time (44 h) after passing through the desilting tunnel without a guiding channel as the reference point. This facilitates comparison of the differences between having and not having a dredged guiding channel. Simulation results from the Typhoon Lupit event indicate that, under terrain conditions with a dredged guiding channel, the velocity required for sediment to reach the entrance of the desilting tunnel is faster and concentrated than without a dredged guiding channel, and the sediment concentration at the entrance is higher. These findings are consistent with the results in Table 6 and Fig. 7.

Table 7 summarizes the simulation results, comparing transportation time, desilting efficiency, and peak concentration ratio for scenarios with and without a dredged guiding channel. Across four reservoir operation strategies, transportation time differences were minimal. When substantial inflow turbidity is released downstream through the desilting tunnel in the midstream section of Nanhua Reservoir, the inflow turbidity reaches the dam site more rapidly in both dredged guiding channel scenarios. However, under conditions with the dredged guiding channel, the inflow turbidity is more concentrated as it approaches the dam, thereby enhancing desilting efficiency across all scenarios. The most significant efficiency improvement occurred in the sluicing operation scenario, while the least impact was observed under free overflow conditions. The dissipation and entrainment effects, as shown by the peak concentration ratios, remained similar across scenarios. Without sediment management using the desilting tunnel or dredged guiding channel, the inflow turbidity took longer to reach the dam site. Simulated desilting efficiency results further indicated that when outflow volumes are similar, the desilting tunnel achieves greater sediment removal efficiency than the spillway.

Table 6
Simulated hydraulic desiltation values.

Cases	Location	Time (hr)	Time difference (hr)	Peak concentration (ppm)	Concentration difference (ppm)
C-1	Measurement location of Sec. 13	7	-1	3816	7401
/C′-1		6		11,218	
	Desilting tunnel	10	-2	2310	8256
		8		10,566	
	Intake at the dam site	15	-1	474	1969
		14		2443	
C-2	Measurement location of Sec. 13	8	-2	4722	6186
/C′-2		6		10,909	
	Desilting tunnel	10	-3	3218	7101
		7		10,319	
	Intake at the dam site	15	-2	332	1657
		13		1990	
C-3	measurement location of Sec. 13	7	-1	4906	6311
/C′-3		6		11,217	
	Desilting tunnel	10	-4	3624	7021
		6		10,646	
	Intake at the dam site	18	-2	238	1625
		16		1863	
C-4	measurement location of Sec. 13	7	-1	3013	8047
/C′-4		6		11,060	
	Desilting tunnel	11	-4	1377	9251
		7		10,627	
	Intake at the dam site	22	-6	312	1853
		16		2165	
C-5	measurement location of Sec. 13	10	-5	4106	7021
/C′-5		5		11,127	
	Desilting tunnel	13	-5	2706	7825
		8		10,532	
	Intake at the dam site	37	-14	372	2832
		23		3204	
C-6	measurement location of Sec. 13	8	-2	4786	5749
/C′-6		6		10,535	
	Desilting tunnel	19	-12	4067	5955
		7		10,022	
	Intake at the dam site	29	-5	451	1646
		24		2097	
Cases	Location	Time (hr)	Time difference (hr)	Peak concentration (ppm)	Concentration difference (ppm)
C-7	Measurement location of Sec. 13	8	-2	4294	6818
/C′-7		6		11,112	
	Desilting tunnel	12	-5	3149	7187
		7		10,336	
	Intake at the dam site	25	-9	416	1368
		16		1784	
C-8	Measurement location of Sec. 13	9	-3	5373	5452
/C′-8		6		10,825	
	Desilting tunnel	14	-7	4142	6188
		7		10,329	
	Intake at the dam site	30	-14	337	1489
		16		1826	
C-9	Measurement location of Sec. 13	8	0	4219	6887
/C′-9		8		11,106	
	Desilting tunnel	15	-7	2503	7952
		8		10,455	
	Intake at the dam site	38	-19	546	1788
		19		2333	
C-10	measurement location of Sec. 13	8	-2	4606	6542
/C′-10		6		11,148	
	Desilting tunnel	20	-13	3315	7404
		7		10,719	
	Intake at the dam site	28	-4	358	1324
		24		1682	
C-11	measurement location of Sec. 13	8	-2	4606	6612
/C′-11		6		11,219	
	Desilting tunnel	12	-5	3149	7354
		7		10,504	
	Intake at the dam site	23	-3	327	1334
		20		1660	

(*continued on next page*)

Table 6 (*continued*)

C-12 /C′-12	measurement location of Sec. 13	11 6	-5	3572 10,878	7306
	Desilting tunnel	13 7	-6	2544 10,433	7889
	Intake at the dam site	34 29	-5	588 1770	1182

4. Conclusions

This study developed, calibrated, and validated a two-dimensional numerical model of Nanhua Reservoir to assess turbidity current dynamics, sediment transport processes, and desilting efficiency under various hydrological conditions. Comparisons with field measurements and hydraulic model test data confirm that the 2DLAM model accurately reproduces sediment concentration evolution, hydrograph behavior, and cumulative sediment discharge during Typhoon Lupit, Typhoon Kalmaegi, and a 25-year return period event. The minor discrepancies in cumulative sediment load—1.63 %, 0.63 %, and –1.01 %, respectively—demonstrate high model reliability and strong agreement with previous research findings (Lai et al., 2015; Huang et al., 2019; Hung et al., 2022; Lee and Du, 2025). Simulated desilting efficiencies ranging from 7.46 % to 25.09 % highlight the dependence of sediment release on inflow discharge and sediment supply. Overall, the validated model provides a robust framework for analyzing turbidity current behavior and optimizing sediment management in Nanhua Reservoir.

The analysis further shows that although empty-reservoir flushing can indicate the general pathway of deep scour, accurate determination of the bottom-guided flow channel's geometry requires higher discharge conditions and extended flushing durations. By simulating a constant inflow of 1000 m^3/s with the desilting tunnel fully open for 120 h, the model successfully delineated the erosion–deposition patterns necessary for designing an effective guiding channel. Consistent with earlier findings (Chen, 2020; Liu, 2023; Imtiyaz et al., 2024; Lee and Huynh Nguyen, 2024), the proposed dredged channel—extending approximately 3.8 km from section 27 to section 10—provides a hydraulically favorable alignment and slope (0.0068) that improves sediment conveyance, particularly through the mid-reservoir S-bend where morphological adjustments are most pronounced. The trapezoidal channel geometry, with a 100 m base width and 130 m top width, offers a structurally and hydraulically coherent configuration for future guiding-channel implementation and reservoir desilting operations.

Event-scale simulations during Typhoon Lupit demonstrate that the dredged guiding channel substantially enhances the delivery of sediment-laden flows to the desilting tunnel. With the guiding channel in place, turbidity currents travel more rapidly and with greater concentration toward the tunnel entrance, thereby improving desilting performance across all operational strategies examined. The most tremendous improvements occur under sluicing operations, while even free-overflow scenarios show quantifiable benefits. Peak concentration ratios indicate similar dissipation and entrainment behavior among scenarios, but the guiding channel consistently reduces lateral spreading and increases sediment discharge efficiency. In contrast, without sediment management structures, turbidity arrival at the dam site is delayed and sediment removal is reduced. The simulations additionally confirm that, under similar outflow volumes, the desilting tunnel provides markedly greater sediment removal than the spillway.

These findings align closely with the "main-channel characteristic" approach applied in previous studies to enhance sediment transport under various water-level conditions (Chen, 2022; Imtiyaz et al., 2024). Under Q5 inflow conditions, this study demonstrates nearly a threefold increase in desilting efficiency when employing a dredged guiding channel. Comparable trends reported by Lee and Huynh Nguyen (2024)—where artificial guiding achieved over 75 % efficiency at low water levels, compared with approximately 65 % without guiding—underscore the broader applicability of guiding measures. Notably, in this study, higher water levels were associated with improvements exceeding fourfold under similar Q5-type conditions. Differences among studies in guiding-channel placement—from the midstream region to areas immediately upstream of the dam (Imtiyaz et al., 2024)—further illustrate how channel geometry and alignment influence performance. Overall, the findings conclusively demonstrate that well-designed dredged guiding channels significantly enhance desilting operations and improve reservoir sediment management outcomes.

The broader implications of this research extend to sediment-laden river–reservoir systems in diverse hydrological and geomorphological settings. The validated two-dimensional modeling framework offers a versatile, practical tool for evaluating desilting strategies, predicting turbidity current behavior, and supporting reservoir operation planning. The observed reduction in sediment concentration during reservoir passage and the strong correlation between inflow and internal sediment levels provide actionable insights into sediment routing and operational timing. The study highlights that strategic adjustments—such as timing desilting tunnel operation during high-inflow periods, optimizing sluicing discharges, and maintaining dredged guiding channels—can substantially improve sediment release efficiency. Integrating hydrodynamic modeling with operational, ecological, and structural considerations will therefore be essential for transitioning toward more adaptive and sustainable reservoir sediment management.

Authors Contributions

Fong-Zuo Lee developed the principal concepts, generated the analyzed data, and wrote the manuscript. Yu-Yun Tu was responsible for simulating cases and editing the framework.

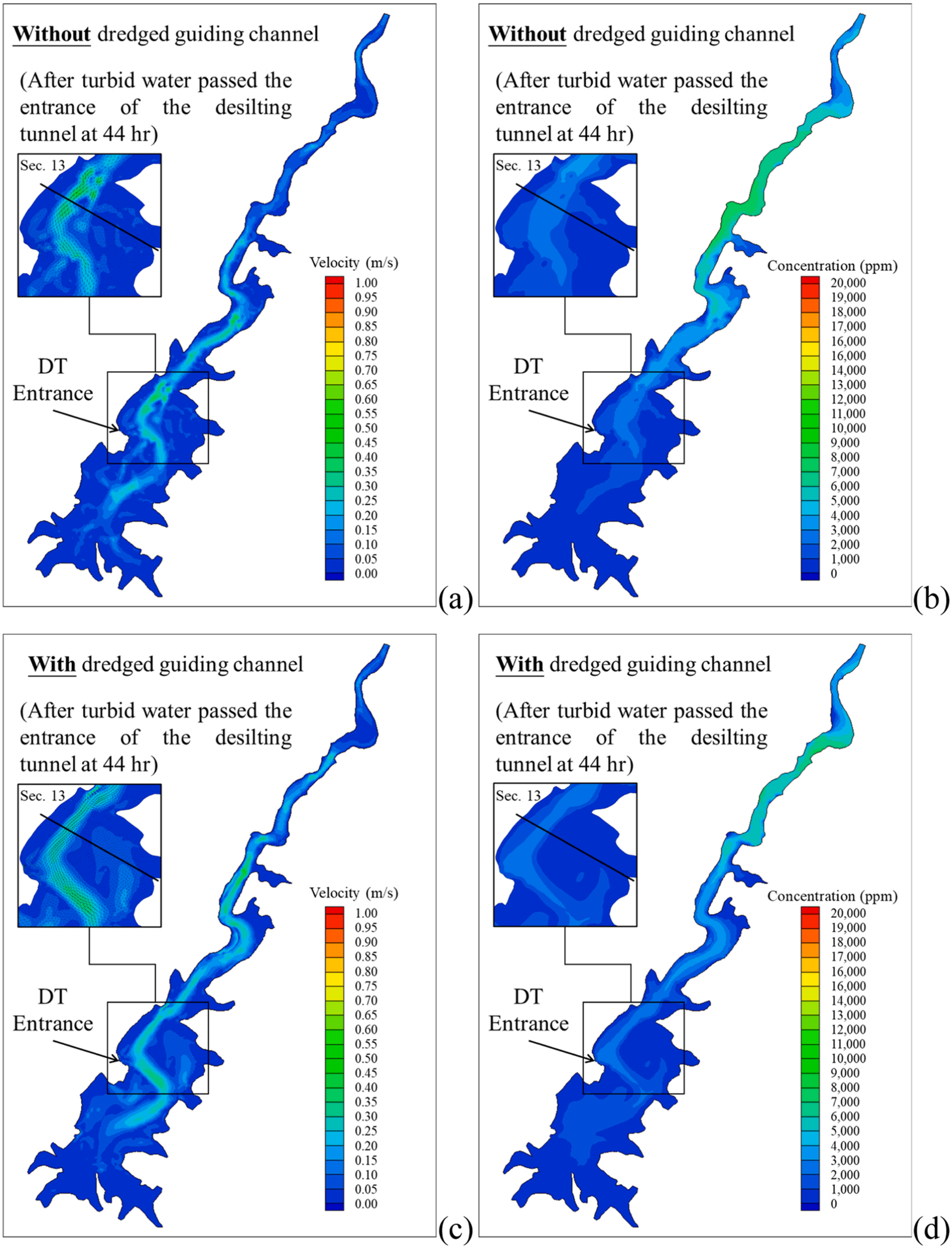

Fig. 8. Flow field (a)velocity distribution without dredged guiding channel, (b)concentration distribution without dredged guiding channel, (c) velocity distribution with dredged guiding channel, (d)concentration distribution with dredged guiding channel.

Table 7
Improvement of transportation time, desilting efficiency, and peak concentration ratio.

Scenarios	Dredged guiding channel	Free overflow (SW)	Downstream replenishment sediment flushing (DT)	Sluicing operation (DT)	Flood mitigation (DT)
Transportation time (hr.) at DT	Without	12.50	11.0	11.0	12.5
	With	8.0	7.0	6.5	7.0
Shorten time (hr.)	Without-With	4.5	4	4.5	5.5
Desilting efficiency (%)	Without	0.96	6.55	4.79	3.14
(Σ(DT/ Guanshan No. 9 Bridge) or(SW/ Guanshan No. 9 Bridge))	With	6.61	16.47	21.26	15.85
Average increasing percentage of desilting efficiency (%)	With/ Without	5.65	9.92	16.47	12.71
Peak concentration ratio (DT/ Guanshan No. 9 Bridge	Without	0.08	0.11	0.10	0.07
or SW/ Guanshan No. 9 Bridge)	With	0.32	0.31	0.32	0.32
Average increase of peak concentration ratio	With/ Without	0.24	0.20	0.22	0.25

CRediT authorship contribution statement

Fong-Zuo Lee: Writing – original draft, Methodology, Investigation, Data curation. **Yu-Yun Tu:** Writing – review & editing, Formal analysis.

Ethical Approval

Not applicable.

Consent to Participate

Not applicable.

Consent to Publish

Not applicable.

Funding

The National Science and Technology Council in Taiwan supported the presented study. The project numbers are NSTC 113–2221-E-005–027, NSTC 113–2625-M-002–018, and NSTC 114–2625-M-002–005.

Declaration of Competing Interest

The authors declare the following financial interests/personal relationships which may be considered as potential competing interests: Fong-Zuo Lee reports financial support was provided by National Science and Technology Council. Not applicable. reports a relationship with Not applicable. that includes:. Not applicable. has patent Not applicable. pending to Not applicable. Not applicable. If there are other authors, they declare that they have no known competing financial interests or personal relationships that could have appeared to influence the work reported in this paper.

Acknowledgment

The author acknowledges the Taiwan Water Corporation for providing the essential data for analysis and simulation. The author also wishes to thank National Taiwan University and the NCKU Research & Development Foundation for manpower and technical support. In addition, the authors acknowledge the Technical Service Center of the United States Bureau of Reclamation for the numerical software used in this study.

Data availability

Data will be made available on request.

References

Albayrak, I., Müller-Hagmann, M., Boes, R., 2019. Efficiency evaluation of Swiss Sediment Bypass Tunnels. Proc. 3rd Int. Workshop Sediment Bypass Tunn. 239–245.

Anari, R., Hotchkiss, R.H., Langendoen, E.J., 2020. Elements for the successful computer simulation of sediment management strategies for reservoirs. Water 12 (3), 714.
Annandale, G.W., Morris, G.L., Karki, P., 2016. Sustainable sediment management for dams and run-of-river hydropower. The World Bank, Washington DC. Extending life Reserv.
Baghalian, S., Ghodsian, M., 2020. Experimental study on the effects of artificial bed roughness on turbidity currents over abrupt bed slope change. Int. J. Sediment Res. 35 (3). Article 3.
Batuca, D.G., Jordaan, J.M., 2000. Silting and Desilting of Reservoirs. Balkema Publishers, Rotterdam.
Chamoun, S., De Cesare, G., Schleiss, A.J., 2017. Management of turbidity current venting in reservoirs under different bed slopes. J. Environ. Manag. 204, 519–530.
Chamoun, S., De Cesare, G., Schleiss, A.J., 2018. Influence of operational timing on the efficiency of venting turbidity currents. J. Hydraul. Eng. 144 (9), 04018062.
Chen, C.N., Tsai, C.H., 2017. Estimating sediment flushing efficiency of a shaft spillway pipe and bed evolution in a reservoir. Water 9 (12), 924.
Chen, P.A., 2022. Integration of multiple outlets' operation and sediment management options in the reservoir for increasing efficiency of turbidity current venting and clear water storages. Doctoral thesis, Kyoto University, Kyoto, Japan.
Chen, S.Y., 2020. Applying the two-dimensional (2D) layer-averaged turbidity current model to estimate outlet sediment concentration and desilting efficiency in the Zengwen Reservoir. Master thesis. National Taiwan University, Taiwan.
De Cesare, G., Boillat, J.L., Schleiss, A.J., 2006. Circulation in stratified lakes due to flood-induced turbidity currents. J. Environ. Eng. 132 (11), 1508–1517.
Engelund, F., Hansen, E., 1972. A monograph on sediment transport in alluvial streams, 0stervoldgade 10. Technical University of Denmark, Copenhagen K.
Esmaeili, T., Sumi, T., Kantoush, S.A., Kubota, Y., Haun, S., Rüther, N., 2021. Numerical study of discharge adjustment effects on reservoir morphodynamics and flushing efficiency: an outlook for the Unazuki reservoir, Japan. Water 13 (12), 1624. https://doi.org/10.3390/w13121624.
Ge, H., Zhu, L., Lin, Q., Deng, C., 2021. Analysis of sediment deposition in Lushui Reservoir to guide dredging. Arab. J. Geosci. 14 (2). Article 2.
Hu, P., Cao, Z., Pender, G., Tan, G., 2012. Numerical modeling of turbidity currents in the Xiaolangdi reservoir, Yellow River, China. J. Hydrol. 464, 41–53.
Huang, C.C., 2024. Navigating reservoir deposition challenges: Evaluation of reservoir desilting strategy through a 4-stage life cycle assessment approach. Water Resour. Manag. 116.
Huang, C.C., Lai, Y.G., Lai, J.S., Tan, Y.C., 2019. Field and numerical modeling study of turbidity current in Shimen Reservoir during typhoon events. J. Hydraul. Eng. 145 (5), 05019003.
Hung, C.C., Lai, J.S., Huang, C.C., 2022. An efficient and economic desilitation strategy for reservoir sustainable development under the extreme flooding threaten. J. Water Clim. Change 13 (3), 1257–1274.
Imtiyaz, N., Lee, F.Z., Lin, G.F., Lai, J.S., 2024. Modeling and analysis of turbidity currents in a reservoir with the dredged guiding channel. KSCE J. Civ. Eng. 1–13.
Kantoush, S.A., Mousa, A., Shahmirzadi, E.M., Toshiyuki, T., Sumi, T., 2021. Pilot Field Implementation of Suction Dredging for Sustainable Sediment Management of Dam Reservoirs. J. Hydraul. Eng. 147 (2). Article 2.
Kondolf, M., Gao, Y., Annandale, G.W., Morris, G.L., Jiang, E., Zhang, J., Cao, Y., Carling, P., Fu, K., Guo, Q., Hotchkiss, R., Peteuil, C., Sumi, T., Wang, H.W., Wang, Z., Wei, Z., Wu, B., Wu, C., Yang, C.T., 2014. Sustainable sediment management in reservoirs and regulated rivers: Experiences from five continents. Earth'S. Future 2, 256–280.
Lai, Y.G., 2010. Two-dimensional depth-averaged flow modeling with an unstructured hybrid mesh. J. Hydraul. Eng. 136 (1), 12–23.
Lai, Y.G., 2015. Advances in geofluvial modeling: methodologies and applications. Adv. Water Resour. Eng. 407–470.
Lai, Y.G., 2017. Modeling stream bank erosion: practical stream results and future needs. Water 2017 9, 950. https://doi.org/10.3390/w9120950.
Lai, Y.G., Huang, J.C., Wu, K.W., 2015. Reservoir turbidity current modeling with a two-dimensional layer-averaged model. J. Hydraul. Eng. 141 (12).
Lai, Y.G., Huang, J., Greimann, B.P., 2024. Hydraulic flushing of sediment in reservoirs: Best practices of numerical modeling. Fluids 9 (2), 38.
Lee, F.Z., Du, Y.Y., 2025. Desilting efficiency assessment under four hydraulic sediment prevention operations. Water Resour. Manag. https://doi.org/10.1007/s11269-025-04161-2.
Lee, F.Z., Huynh Nguyen, N.L., 2024. Application of artificial countermeasures to enhance desilting efficiency in a reservoir under normal and extreme events. J. Water Clim. Change 15 (6), 2648–2664.
Lee, F.Z., Lai, J.S., Tan, Y.C., Sung, C.C., 2014. Turbid density current venting through reservoir outlets. KSCE J. Civ. Eng. 18 (2), 694–705.
Lee, F.Z., Huang, M.S., Liu, C.C., Song, D.R., Liu, R., Chiueh, P.T., 2021. Application of 2-D numerical model on flood control and sediment transportation for barrage types. J. Taiwan Agric. Eng. 67 (2), 32–43.
Lee, F.Z., Liu, C.C., Lai, J.S., Chiueh, P.T., 2023. Study on the application of flushing channel with guide wall to reduce sedimentation in a reservoir. J. Taiwan Agric. Eng. 69 (2), 11–21.
Lee, F.Z., Lai, J.S., Kantoush, S.A., Sumi, T., 2024. 2024. Analysis of turbidity current plunging and floating woody debris in a reservoir during flood events. J. Hydrol. Reg. Stud. 56, 1–15, 102027.
Liu, C.C., 2023. Influences of the Reservoir Desiltation on the Risk of Water Supply Operation. Master Thesis, Graduate Institute of Environmental Engineering, College of Engineering. National Taiwan University (In Chinese).
Morris, G.L., 2020. Classification of management alternatives to combat reservoir sedimentation. Water 12 (3). Article 3.
Morris, G.L., Fan, J., 2010. Reservoir Sedimentation Handbook. Electronic version. McGraw-Hill Book Co, New York. Ver. 1.04.
Oehy, C.D., Schleiss, A.J., 2007. Control of turbidity currents in reservoirs by solid and permeable obstacles. J. Hydraul. Eng. 133 (6), 637–648.
Robb, D.M., Pieters, R., Lawrence, G.A., 2021. Fate of turbid glacial inflows in a hydroelectric reservoir. Environ. Fluid Mech. 21 (6), 1201–1225.
Samad, N., Chauhdry, M.H., Ashraf, M., Saleem, M., Hamid, Q., Babar, U., Tariq, H., Farid, M.S., 2016. Sediment yield assessment and identification of check dam sites for Rawal Dam catchment. Arab. J. Geosci. 9 (6). Article 6.
Sun, Y., Li, J., Cao, Z., Borthwick, A.G., Józsa, J., 2023. Effect of tributary inflow on reservoir turbidity current. Environ. Fluid Mech. 23, 259–290.
Taiwan Water Corporation Sixth Branch, 2017. . Tainan, Taiwan. (In Chinese)Hydraulic Model Test of Flood and Sediment Prevention Sub-Dam and Empty Reservoir Flushing for the Nanhua Reservoir.
Taiwan Water Corporation Sixth Branch, 2021. . Tainan, Taiwan. (In Chinese)Research on the establishment and application of a turbidity monitoring system for the Nanhua Reservoir inflow.
Taiwan Water Corporation Sixth Branch, 2023a. . Tainan, Taiwan. (In Chinese)2023Nanhua Reservoir Sedimentation Survey.
Taiwan Water Corporation Sixth Branch, 2023b. . Tainan, Taiwan. (In Chinese)Nanhua Reservoir Operation Decision Support and Sediment Transport Monitoring.
Wang, H.W., Tsai, B.S., Hwang, C., Chen, G.W., Kuo, W.C., 2020. Efficiency of the drawdown flushing and partition desilting of a reservoir in Taiwan. Water 12 (8), 2166.
WRA, 2014. . Taipei, Taiwan.Hydraulic Model Test of Sediment Desilting Project for the Nanhua ReservoirIn Chinese.
WRA, 2020. . Taipei, Taiwan.Sediment observation for desiltation of Agongdian Reservoir by using empty flushing and consultation for flood control operation in 2020.
Zeng, Y., Meng, X., Zhang, Y., Dai, W., Fang, N., Shi, Z., 2022. Estimation of the volume of sediment deposited behind check dams based on UAV remote sensing. J. Hydrol. 612, 128143.
Zulfan, J., Ginting, B., Rimawan, R., 2023. Assessment of reservoir sedimentation and mitigation measures using 2D hydrodynamic modeling: Case study of Pandanduri Reservoir, Indonesia. IOP Conference Series Earth Environmental Science.